Deadbeat Control Based on a Multipurpose Disturbance Observer for Permanent Magnet Synchronous Motors

Haitao Yang[1], Yongchang Zhang[2,*], Jiejunyi Liang[1], Bo Xia[2] Paul D. Walker[1], and Nong Zhang[1]

[1]Faculty of Engineering and Information Technology, University of Technology, Sydney, NSW 2007, Australia.

[2]Inverter Technologies Engineering Research Center of Beijing, North China University of Technology, Beijing 100144, China.

* zhangdavid37@gmail.com

Abstract

Robustness against parameter mismatches and position-sensorless operation are two important research topics for permanent magnet synchronous motor (PMSM) drives. In this paper, a sliding mode disturbance observer (SMDO) is proposed to achieve either of two functions for different application environments: 1) if a position sensor is equipped, accurate current regulation can be achieved by deadbeat predictive current control (DBPC) despite mismatched motor parameters; 2) if the position sensor is not equipped but with a good estimation of motor parameters, the observer can serve as a back electromotive force (EMF) estimator. On this basis, the rotor position can be extracted for position-sensorless control. Usually, low-pass filter is required to suppress high frequency noises in conventional sliding mode observer. This inevitably leads to phase delay in the estimation, which cannot be directly used for disturbance compensation. While in the proposed method, a complex coefficient filter is inherently embedded, which can provide accurate estimation without phase or magnitude error. Experimental results obtained from a 2.4 kW PMSM drive platform indicate that high performance current control can be achieved with good robustness for position sensor based operation. And, rotor position can be accurately estimated with good steady and dynamic performance for position-sensorless operation.

Deadbeat Control Based on a Multipurpose Disturbance Observer for Permanent Magnet Synchronous Motors

I. Introduction

For power converters and motor drives, inner current loop plays an important role in performance of the whole control system. During past decades, many methodologies have been investigated for high performance current regulation, including proportional-integral (PI) control [1], [2], hysteresis control [3], [4], sliding-mode control [5], and predictive control [6]–[8].

PI control is widely used in practical applications due to its simplicity and good steady state performance. However, to reduce overshoot during dynamic process and attenuate interference with sampling noise, the bandwidth of such controller is usually limited and hard to tune [9]. Additionally, classic PI control may suffer from instability during high speed operation [1]. Hysteresis control presents fast dynamic response and good robustness. The main issues are requirement of high sampling frequency, relatively larger current ripples and variable switching frequency. Sliding-mode control (SMC) features good robustness against disturbance and dynamic performance [10]. In practical application, SMC must be well designed to avoid high frequency chattering. Generally, predictive control can be classified into finite-control-set control (FCSC) and continuous-control-set control (CCSC). In FCSC, there is no modulator and the discrete voltage vector is directly selected online by minimizing a cost function [11], [12]. FCSC has advantages of fast dynamic response and flexibility to handle system constrains, etc. However, the computational burden of FCSC is usually high especially for long prediction horizons [13] and multiple vectors based schemes [14]. Additionally, variable switching frequency and relatively larger harmonic ripples are issues need to be addressed. In CCSC, the output voltage is usually synthesized by a modulator with fixed switching frequency and concentrated harmonic spectrum. Among CCSCs, deadbeat predictive control (DBPC) is one of the commonly used methods owing to its good dynamic performance and simple calculation. However, as DBPC is directly derived based on the system model to cancel tracking error at the next sampling instant, its performance is inevitably influenced by accuracy of model parameters.

To achieve satisfactory performance based on crude estimation of system models, many methods have been proposed for model based predictive control. In [15], a predictive current control based on an extended Luenberger observer is investigated for the current control of PWM rectifier. By compensating the estimated disturbances in predictive model, the tracking error is effectively eliminated during steady state. Similarly, a sliding mode observer with an improved reaching law is proposed in [6] for robust current control of PMSMs. These methods are designed in synchronous reference frame, which requires position information for proper implementation. Hence, such observers cannot be directly used for position-sensorless control. In [16], a closed-loop prediction model with

sliding mode feedback is proposed for sensorless control of induction motor drives. By designing feedback gains based on H-∞ methods, good performance is obtained with uncertain stator and rotor resistances. For finite-control-set predictive current control of PMSMs, a simple yet very effective method by adding prediction error for all voltage vectors is studied in [7]. The demonstrated results show that the current ripples are reduced and the robustness against inductance variation is improved.

To achieve high performance current control of PMSMs, accurate information of rotor position is usually required. In practice, position-sensorless operation is preferred in hostile environments and low cost applications [17], [18]. Even equipped with a position sensor, a rotor position estimator is still required to achieve sensor fault-tolerant control for safety or reliability reason in some cases, such as in automotive applications [19]. For position-sensorless control of PMSMs, many model based methods can be found in existing literature. In [20], some design principles are introduced to improve stability and dynamic performance of full order observer (FOO). To reduce the sensitivity of extended Kalman filter (EKF) to round-off errors, different square-root algorithms based EKFs are studied and compared in [21]. Apart from FOO and EKF, sliding mode observer (SMO) has also been widely used because of its simplicity and satisfactory performance [18], [22], [23]. The main issues of SMO in practical application include high frequency chattering and harmonic ripples in estimated position caused by inverter nonlinearity and flux spatial harmonics, etc. To obtain smooth rotor position, different filters can be used to filter out harmonic components [24].

Usually, previous observers are specially investigated for "single-use". Few research investigates using one observer to meet requirements for different application environments. For a compact solution, a sliding-mode disturbance observer (SMDO) is designed in this paper, which can be used for different purposes. The main contributions include:

1) A SMDO is designed and investigated for robustness against parameter variation and sensorless control. If rotor position is measured, the observer can provide precise compensation of unknown disturbance caused by mismatched parameters. In this case, its function is similar to that in [6], [15]. If rotor position needs to be estimated, the position can be extracted from the estimated disturbance. In this case, its function is similar to that in [22], [23], which can provide rotor position for coordinate transformation.
2) For compact representation and to facilitate theoretical analysis, complex-vector based state variables rather than conventional scalar notations are used for stability and performance analysis of SMDO.
3) A complex-coefficient filter is inherently incorporated in the designed SMDO, which can preserve fundamental components while suppressing harmonics. Neither low pass filter nor phase compensation is required.
4) Both robustness of control system and sensorless operation are experimentally evaluated on a two-level inverter fed PMSM drive. The obtained results confirm that two functions can be achieved in one design.

II. Model of PMSM and Basic Principle of DBPC

A. Mathematical Equations of PMSM

In the stationary $\alpha - \beta$ reference frame, the motor equation of a surface-mounted PMSM can be written in the form of complex-vectors as

$$L_s \frac{d\boldsymbol{i}_s}{dt} = \left(\boldsymbol{u}_s - R_s \boldsymbol{i}_s - j\omega_r \psi_r e^{j\theta_r}\right). \tag{1}$$

where $\boldsymbol{u}_s = u_{s\alpha} + j \cdot u_{s\beta}$, $\boldsymbol{i}_s = i_{s\alpha} + j \cdot i_{s\beta}$ are stator voltage and stator current vectors; R_s and L_s are stator resistance and inductance; ω_r is electrical rotor speed; ψ_r represents rotor flux magnitude of permanent magnet; θ_r is rotor position; and j represents imaginary component of a complex variable. With a small sampling period T_{sp}, (1) can be discretized by the following simple Euler method

$$\frac{dx}{dt} \approx \frac{x^{k+1} - x^k}{T_{sp}} \tag{2}$$

as

$$\boldsymbol{i}_s^{k+1} = \boldsymbol{i}_s^k + \frac{T_{sp}}{L_s}(\boldsymbol{u}_s^k - R_s \boldsymbol{i}_s^k - j\omega_r^k \psi_r e^{j\theta_r^k}). \tag{3}$$

where the superscript k represents kth sampling instant.

B. Basic Principle of DBPC

To force stator current to reach its reference at the next sampling instant, i.e. $\boldsymbol{i}_s^{k+1} = \boldsymbol{i}_{ref}^{k+1}$, the applied stator voltage $\boldsymbol{u}_s^k$ should be

$$\boldsymbol{u}_s^k = L_s \frac{\boldsymbol{i}_{ref}^{k+1} - \boldsymbol{i}_s^k}{T_{sp}} + R_s \boldsymbol{i}_s^k + j\omega_r^k \psi_r e^{j\theta_r^k}. \tag{4}$$

In digital implementation, there is typically one-step delay between the actual applied voltage and the calculated voltage [25]. This means that the calculated $\boldsymbol{u}_s^k$ will be applied in the $(k+1)$th instant in practical application rather than the expected kth instant. In this paper, model based prediction is employed to compensate for digital delay. By further shifting (4) one-step ahead, $\boldsymbol{u}_s^{k+1}$ can be solved as

$$\boldsymbol{u}_s^{k+1} = L_s \frac{\boldsymbol{i}_{ref}^{k+2} - \boldsymbol{i}_s^{k+1}}{T_{sp}} + R_s \boldsymbol{i}_s^{k+1} + j\omega_r^{k+1} \psi_r e^{j\theta_r^{k+1}} \tag{5}$$

where $\boldsymbol{i}_s^{k+1}$ can be predicted based on (3) with stator voltage $\boldsymbol{u}_s^k$ obtained from previous control period. $\boldsymbol{i}_{ref}^{k+2}$ is expressed as

$$\boldsymbol{i}_{ref}^{k+2} = (i_{dref}^{k+2} + j \cdot i_{qref}^{k+2}) e^{j\theta_r^{k+2}}. \tag{6}$$

As filed-weakening operation is not discussed here, i_{dref} is kept as zero and i_{qref} is obtained from outer speed control loop. Considering the bandwidth of outer speed control loop is generally much smaller than the sampling frequency of the inner control loop, it is reasonable to assume that $i_{qref}^{k+2} = i_{qref}^k$. And, θ_r^{k+2} can be extrapolated as $\theta_r^{k+2} = \theta_r^k + 2\omega_r^k T_{sp}$ assuming that ω_r is constant within prediction horizons [13]. Hence, $\boldsymbol{i}_{ref}^{k+2}$ can be simply calculated according to (6) as

$$\boldsymbol{i}_{ref}^{k+2} = j \cdot i_{qref}^k e^{j(\theta_r^k + 2\omega_r^k T_{sp})}. \tag{7}$$

As can be seen from (5), the accuracy of calculated voltage depends on motor parameters. Any deviation in these parameters will deteriorate control performance, which will be discussed in the next section.

III. Impact of Parameter Errors on DBPC

In practical application, the actual values of inductance and resistance are unknown and the output voltage $\boldsymbol{u}_s^{k+1}$ of DBPC can only be calculated based on the estimated motor parameters, measured/estimated position and speed. According to (3) and (5), the final implementation of DBPC in a digital processor can be summarized by the following two equations.

$$\hat{\boldsymbol{i}}_s^{k+1} = \boldsymbol{i}_s^k + \frac{T_{sp}}{\hat{L}_s}(\boldsymbol{u}_s^k - \hat{R}_s \boldsymbol{i}_s^k - j\omega_r^k \hat{\psi}_r e^{j\theta_r^k}) \tag{8}$$

$$\boldsymbol{u}_s^{k+1} = \hat{L}_s \frac{\boldsymbol{i}_{ref}^{k+2} - \hat{\boldsymbol{i}}_s^{k+1}}{T_{sp}} + \hat{R}_s \hat{\boldsymbol{i}}_s^{k+1} + j\omega_r^k \hat{\psi}_r e^{j(\theta_r^k + \omega_r^k T_{sp})}. \tag{9}$$

where the hat $\hat{}$ denotes the estimated variables. If T_{sp}^2 related terms are not considered, the following equations can be obtained according to (50) and (51) deduced in the Appendix.

$$\begin{aligned} L_s i_d^{k+2} = {} & \hat{L}_s i_{dref}^k + (\frac{\hat{R}_s}{\hat{L}_s}\Delta L - \Delta R) T_{sp} i_d^{k+1} \\ & + (\Delta L - \frac{\hat{R}_s}{\hat{L}_s}\Delta L \cdot T_{sp} - \Delta R \cdot T_{sp}) i_d^k \\ & + 2\Delta L \omega_r T_{sp} \cdot i_q^k \end{aligned} \tag{10}$$

$$\begin{aligned} L_s i_q^{k+2} = {} & \hat{L}_s i_{qref}^k + T_{sp}(\frac{\hat{R}_s}{\hat{L}_s}\Delta L - \Delta R) i_q^{k+1} \\ & + (\Delta L - \frac{\hat{R}_s}{\hat{L}_s}\Delta L \cdot T_{sp} - \Delta R \cdot T_{sp}) i_q^k \\ & - 2\omega_r T_{sp} \cdot (\Delta\psi + \Delta L i_d^k) \end{aligned} \tag{11}$$

where $\Delta L = L_s - \hat{L}_s$, $\Delta R = R_s - \hat{R}_s$ and $\Delta\psi = \psi_r - \hat{\psi}_r$ are estimation errors of motor parameters. As $i_d^{k+2} \approx i_d^{k+1} \approx i_d^k$ and $i_q^{k+2} \approx i_q^{k+1} \approx i_q^k$ during steady state, (10) and (11) can be simplified as

$$i_d \approx \frac{\hat{L}_s i_{dref}^k + 2\Delta L \omega_r T_{sp} i_q}{\hat{L}_s + 2\Delta R T_{sp}} \tag{12}$$

$$i_q \approx \frac{\hat{L}_s i_{qref}^k - 2\omega_r T_{sp}(\Delta\psi + \Delta L i_d)}{\hat{L}_s + 2\Delta R T_{sp}}. \tag{13}$$

It can be seen that error of inductance would introduce cross coupling between i_d and i_q. With a small sampling period T_{sp}, $\Delta R T_{sp}$ is generally negligible and thus resistance variation usually has little impact on control performance [7]. The error of rotor flux mainly influences tracking accuracy of $q-$axis current, especially at high speed. Additionally, experimental results in some research [7] show that a over estimated inductance would cause significant larger ripples in the current response. The reason can be explained as follows. When only inductance error is considered, the transfer function (14) can be obtained based on (10) and (11) as

$$H(z) = \frac{i_{dq}(z)}{i_{dq}^{ref}(z)} = \frac{\hat{L}_s}{L_s z^2 - \frac{R_s}{\hat{L}_s}\Delta L T_{sc} \cdot z - \Delta L + \frac{R_s}{\hat{L}_s}\Delta L T_{sc}}. \tag{14}$$

where z is delay operator in discrete-time domain. Fig. 1 shows bode diagram of $H(z)$ with 10 kHz sampling frequency when $\hat{L}_s$ varies from $0.5L_s$ to $2L_s$. It is clear that a overestimated $\hat{L}_s$ would amplify high frequency

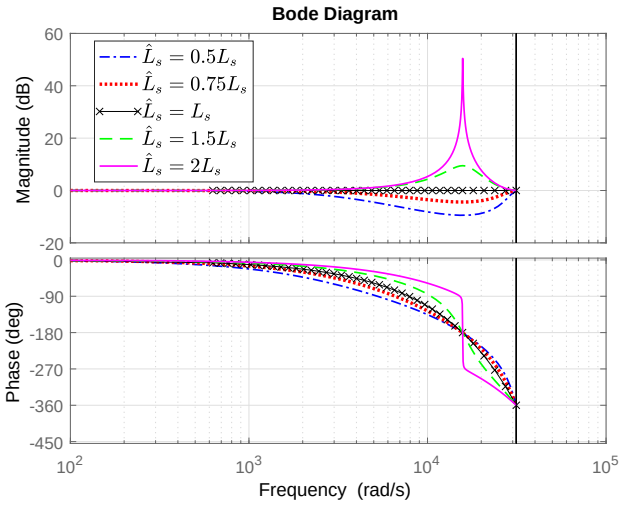

Fig. 1. Bode plot of $H(z)$ in (14) with $\hat{L}_s$ varies from $0.5L_s$ to $2L_s$

noises. In short, inaccurate motor parameters have side-effects on the control performance for conventional DBPC, which needs to be compensated to improve tracking accuracy.

IV. Sliding-Mode Disturbance Observer

A. Disturbance Estimation

From (1), the system model can be rewritten in terms of the estimated inductance $\hat{L}_s$ and resistance $\hat{R}_s$ as

$$\hat{L}_s \frac{d\boldsymbol{i}_s}{dt} = \boldsymbol{u}_s + \boldsymbol{u}_d - \hat{R}_s \boldsymbol{i}_s. \tag{15}$$

where $\boldsymbol{u}_d$ is the disturbance voltage as shown in (16). In (15), $\boldsymbol{u}_d$ is incorporated to compensate for the influence of inaccurate model parameters so that the responses of (15) is exactly the same as (1).

$$\boldsymbol{u}_d = -\Delta L \frac{d\boldsymbol{i}_s}{dt} - \Delta R_s \boldsymbol{i}_s - j\omega_r \psi_r e^{j\theta_r}. \tag{16}$$

From (16), one can see that $\boldsymbol{u}_d$ consists of disturbance resulted from parameter mismatches and back electromotive force (EMF) $j\omega_r \psi_r e^{j\theta_r}$. It is clear that the derivative of $\boldsymbol{u}_d$ is $d\boldsymbol{u}_d/dt = j\omega_r \boldsymbol{u}_d$ when only fundamental component is considered during steady state. Hence, the dynamics of $\boldsymbol{u}_d$ can be expressed as

$$\frac{d\boldsymbol{u}_d}{dt} = j\omega_r \boldsymbol{u}_d. \tag{17}$$

As $\boldsymbol{u}_d$ is not directly available, a sliding-mode disturbance observer (SMDO) is designed based on (15) and (17) as follows.

$$\hat{L}_s \frac{d\hat{\boldsymbol{i}}_s}{dt} = \boldsymbol{u}_s + \hat{\boldsymbol{u}}_d + \boldsymbol{u}_{smo} - \hat{R}_s \hat{\boldsymbol{i}}_s \tag{18}$$

$$\frac{d\hat{\boldsymbol{u}}_d}{dt} = j\omega_r \hat{\boldsymbol{u}}_d + \omega_c \boldsymbol{u}_{smo} \tag{19}$$

where $\boldsymbol{u}_{smo}$ is sliding-mode control function; $\hat{\boldsymbol{u}}_d$ is estimation of the real disturbance voltage $\boldsymbol{u}_d$ and ω_c is the adaption gain for $\hat{\boldsymbol{u}}_d$. Unlike conventional sliding mode observer, the estimated disturbance is not directly

reconstructed from switching function but extracted from sliding mode control function $\boldsymbol{u}_{smo}$ as shown in (19). This can help to attenuate harmonic ripples which will be discussed later. In this paper, sliding-mode surface is chosen as current tracking error, i.e.,

$$\boldsymbol{S} = \boldsymbol{i}_s - \hat{\boldsymbol{i}}_s. \tag{20}$$

To improve dynamic performance and reduce high frequency chattering, the following exponential law (21) is used to design sliding-mode control function [26].

$$\frac{d\boldsymbol{S}}{dt} = -\lambda \cdot \text{sgn}(\boldsymbol{S}) - l \cdot \boldsymbol{S} \tag{21}$$

where λ and l are positive parameters and

$$\text{sgn}(\boldsymbol{S}) = \frac{\boldsymbol{S}}{|\boldsymbol{S}|}. \tag{22}$$

Subtracting (18) from (15) results in the following error dynamics

$$\hat{L}_s \frac{d\boldsymbol{e}_i}{dt} = \boldsymbol{e}_u - \boldsymbol{u}_{smo} - \hat{R}_s \boldsymbol{e}_i. \tag{23}$$

where $\boldsymbol{e}_i = \boldsymbol{S} = \boldsymbol{i}_s - \hat{\boldsymbol{i}}_s$ and $\boldsymbol{e}_u = \boldsymbol{u}_d - \hat{\boldsymbol{u}}_d$. From (21) and (23), equation (24) can be deduced.

$$-\hat{L}_s(\lambda \cdot \text{sgn}(\boldsymbol{S}) + l \cdot \boldsymbol{S}) = \boldsymbol{e}_u - \boldsymbol{u}_{smo} - \hat{R}_s \cdot \boldsymbol{S}. \tag{24}$$

Considering $\boldsymbol{e}_u$ as disturbance, the sliding-mode control function $\boldsymbol{u}_{smo}$ can be derived from (24) as

$$\boldsymbol{u}_{smo} = \hat{L}_s \lambda \cdot \text{sgn}(\boldsymbol{S}) + (\hat{L}_s l - \hat{R}_s) \cdot \boldsymbol{S}. \tag{25}$$

B. Analysis of SMDO

To investigate stability of SMDO, the following Lyapunov function is defined.

$$F = \frac{|\boldsymbol{S}|^2}{2} = \frac{\boldsymbol{S} \odot \boldsymbol{S}}{2} \tag{26}$$

where $\odot$ represents dot product of two complex variables. The time derivative of F is

$$\dot{F} = \dot{\boldsymbol{S}} \odot \boldsymbol{S} \tag{27}$$

The error of estimated current $\boldsymbol{e}_i$ will always approach zero if

$$\dot{F} = \dot{\boldsymbol{S}} \odot \boldsymbol{S} = \dot{\boldsymbol{e}}_i \odot \boldsymbol{e}_i < 0. \tag{28}$$

To ensure stability of SMDO, the parameter λ, l and ω_c must be properly designed so that (28) is always satisfied. Based on (23) and (25), the condition (28) can be written as

$$\dot{F} = \frac{\boldsymbol{e}_u \odot \boldsymbol{e}_i}{\hat{L}_s} - \lambda \cdot |\boldsymbol{e}_i| - l\,|\boldsymbol{e}_i|^2 < 0. \tag{29}$$

As $\boldsymbol{e}_u \odot \boldsymbol{e}_i < |\boldsymbol{e}_u| \cdot |\boldsymbol{e}_i|$, to ensure $\dot{F} < 0$, λ and l can be selected as

$$\lambda > \frac{|\boldsymbol{e}_u|}{\hat{L}_s} \tag{30}$$

$$l > 0. \tag{31}$$

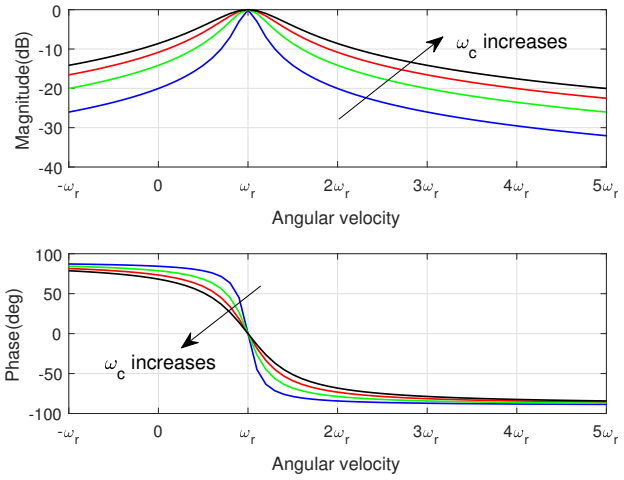

Fig. 2. Bode plot of $G(s)$ in (33) when ω_c increase from $0.1\omega_r$ to $0.4\omega_r$.

With parameters chosen based on (30) and (31), the stability of SMDO can be guaranteed.

After stability study, the equivalent relationship between $\hat{\boldsymbol{u}}_d$ and $\boldsymbol{u}_d$ when state variables move along sliding surface is derived for analysis of steady-state performance. As $\boldsymbol{S} = 0$ when SMO stays on sliding surface, (24) can be simplified as

$$\boldsymbol{u}_{smo} = \boldsymbol{e}_u = \boldsymbol{u}_d - \hat{\boldsymbol{u}}_d \tag{32}$$

Based on (19) and (32), the following transfer function can be obtained

$$G(s) = \frac{\hat{\boldsymbol{u}}_d(s)}{\boldsymbol{u}_d(s)} = \frac{\omega_c}{s - j\omega_r + \omega_c} \tag{33}$$

As $G(j\omega_r) = 1$, $\hat{\boldsymbol{u}}_d$ can track the fundamental component of $\boldsymbol{u}_d$ without any phase or magnitude error during steady state. The bode diagram of $G(s)$ is shown in Fig. 2. It is seen that low order and high frequency harmonics can be well attenuated. Hence, a smooth estimation of disturbance can be obtained through designed observer.

C. Discrete-time implementation

By employing first-order Euler method, the aforementioned SMDO as described by equations (18), (19) and (25) can be written as

$$\boldsymbol{u}_{smo}^k = \hat{L}_s\lambda \cdot \text{sgn}\left(\boldsymbol{i}_s^k - \hat{\boldsymbol{i}}_s^k\right) + (\hat{L}_s l - \hat{R}_s) \cdot \left(\boldsymbol{i}_s^k - \hat{\boldsymbol{i}}_s^k\right) \tag{34}$$

$$\hat{\boldsymbol{i}}_s^{k+1} = \hat{\boldsymbol{i}}_s^k + \frac{T_{sp}}{\hat{L}_s}(\boldsymbol{u}_s^k + \hat{\boldsymbol{u}}_d^k + \boldsymbol{u}_{smo}^k - R_s\hat{\boldsymbol{i}}_s^k) \tag{35}$$

$$\hat{\boldsymbol{u}}_d^{k+1} = \hat{\boldsymbol{u}}_d^k + \left(j\omega_r\hat{\boldsymbol{u}}_d^k + \omega_c\boldsymbol{u}_{smo}^k\right)T_{sp}. \tag{36}$$

It can be seen that the final implementation of SMDO in digital processor is relatively simple. To ensure condition (30) is satisfied, λ must be selected large enough on one hand but may increase chattering level in the estimated current on the other hand. To solve this dilemma, λ can be adapted online as

$$\lambda = \lambda_{min} + \frac{|\boldsymbol{e}_u|}{\hat{L}_s} \tag{37}$$

In this way, not only stability condition is satisfied but also λ will approach to a smaller value λ_{min} during steady state when $\boldsymbol{e}_u$ converges to zero. $|\boldsymbol{e}_u|$ can be estimated based on (23) as

$$\boldsymbol{e}_u = \hat{L}_s \frac{\boldsymbol{e}_i^k - \boldsymbol{e}_i^{k-1}}{T_{sp}} + \boldsymbol{u}_{smo}^{k-1} + \hat{R}_s \boldsymbol{e}_i^{k-1} \tag{38}$$

Additionally, switching function sgn($\bullet$) can be approximately rearranged as follows to reduce noise sensitivity and high frequency chattering.

$$\text{sgn}\left(\boldsymbol{i}_s^k - \hat{\boldsymbol{i}}_s^k\right) = \frac{\boldsymbol{i}_s^k - \hat{\boldsymbol{i}}_s^k}{\left|\boldsymbol{i}_s^k - \hat{\boldsymbol{i}}_s^k\right| + \rho} \tag{39}$$

where ρ is a small positive value. To attenuate chattering during steady-state operation, it can be set slightly larger than peak value of sampling noises. In this paper, it is set as $\rho = 0.2$. With (23), (25) and (39), the following transfer function can be obtained.

$$H(s) = \frac{\boldsymbol{e}_i(s)}{\boldsymbol{e}_u(s)} = \frac{1}{\hat{L}_s} \frac{1}{s + \frac{\lambda}{|\boldsymbol{e}_i| + \rho} + l} \tag{40}$$

where s is Laplace operator. From (40), it can be seen that estimation error of stator current is low-pass filtered value of estimation error of $\boldsymbol{e}_u$. The bandwidth of $H(s)$ is

$$\omega_H = \frac{\lambda}{|\boldsymbol{e}_i| + \rho} + l. \tag{41}$$

In conventional SMDO, ρ is zero. This leads to an extremely large ω_H when $|\boldsymbol{e}_i| \approx 0$. The system is thus very sensitive to high frequency noises during steady-state. In reaching law (21), parameter l related proportional rate reaching term is employed for faster converging rate when $|\boldsymbol{e}_i|$ is large. It can be seen that the minimum bandwidth of $H(s)$ is $\omega_H = l$. When $|\boldsymbol{e}_i|$ gets smaller, the constant rate reaching term $\lambda \cdot \text{sgn}(\boldsymbol{e}_i)$ gradually dominates error dynamics. Considering $|\boldsymbol{e}_i| \approx 0$ and $\lambda \approx \lambda_{min}$ during steady-state operation, the maximum bandwidth would be approximately $l + \lambda/\rho$. For a trade-off between dynamic performance and noise immunity, l and λ_{min} are chosen as 1200 and 800 respectively in this paper. With the selected parameters, it is shown in the Section VI that the proposed SMDO achieves satisfactory steady and dynamic performance.

V. Deadbeat Current Control With SMDO

Fig. 3 shows the control diagram of DBPC based on the proposed SMDO. The rotor speed is regulated by a PI controller, from which the $q-$axis current reference i_{qref} is obtained. The rotor position can be either measured or estimated. If rotor position is directly measured, a robust DPBC with satisfactory current tracking performance can be constructed in spite of mismatched motor parameters. If position-sensorless control is required, the proposed SMDO can be used as a position estimator. The details will be explained below.

A. Robust DPBC Based On SMDO

Similar to the deduction of (5), the deadbeat solution of output voltage $\boldsymbol{u}_s^{k+1}$ can be derived based on (15) as

$$\boldsymbol{u}_s^{k+1} = \hat{L}_s \frac{\boldsymbol{i}_{ref}^{k+2} - \boldsymbol{i}_s^{k+1}}{T_{sp}} + \hat{R}_s \boldsymbol{i}_s^{k+1} - \boldsymbol{u}_d^{k+1}. \tag{42}$$

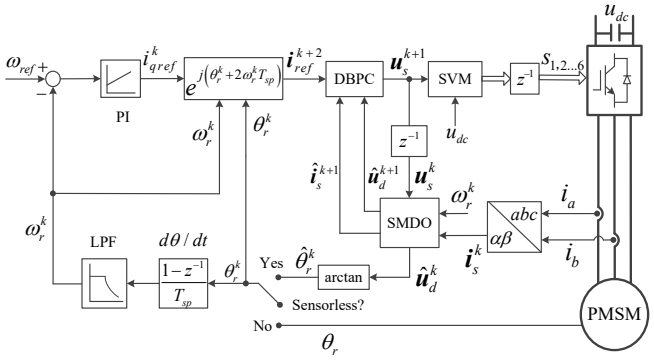

Fig. 3. Control diagram of SMDO based DBPC.

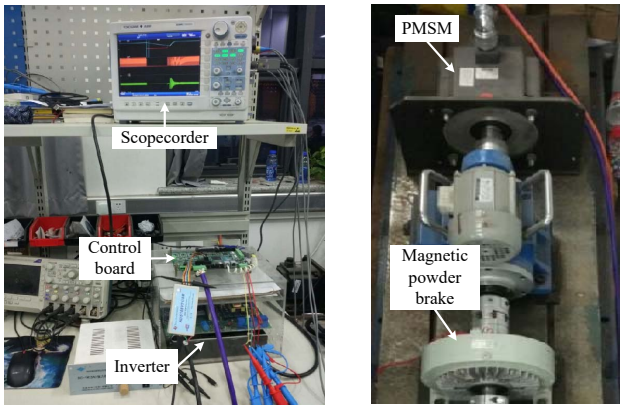

Fig. 4. Experimental setup.

As $\boldsymbol{i}_s^{k+1}$ and $\boldsymbol{u}_d^{k+1}$ are unknown variables, they are replaced by the estimated $\hat{\boldsymbol{i}}_s^{k+1}$ and $\hat{\boldsymbol{u}}_d^{k+1}$ shown in equations (35) and (36) respectively. Analysis in the previous section has proven that the designed SMDO can track actual current and disturbance voltage accurately and thus the solution of (42) would be more robust against parameter mismatches than conventional solution (9).

B. Position Estimation Based On SMDO

With sophisticated offline commissioning, such as the method presented in [27], prior knowledge of stator resistance and inductance can be obtained with good accuracy. Assuming that $\Delta L = 0$ and $\Delta R = 0$, then the disturbance voltage $\boldsymbol{u}_d$ only contains Back EMF as can be seen from (16), namely

$$\boldsymbol{u}_d = -j\omega_r\psi_r e^{j\theta_r} = \omega_r\psi_r\left(\sin(\theta_r) - j\cos(\theta_r)\right) \tag{43}$$

According to (43), the rotor position can be estimated based on $\hat{\boldsymbol{u}}_d$ as

$$\hat{\theta}_r = \arctan\left(\frac{\hat{u}_{d\alpha}}{-\hat{u}_{d\beta}}\right) \tag{44}$$

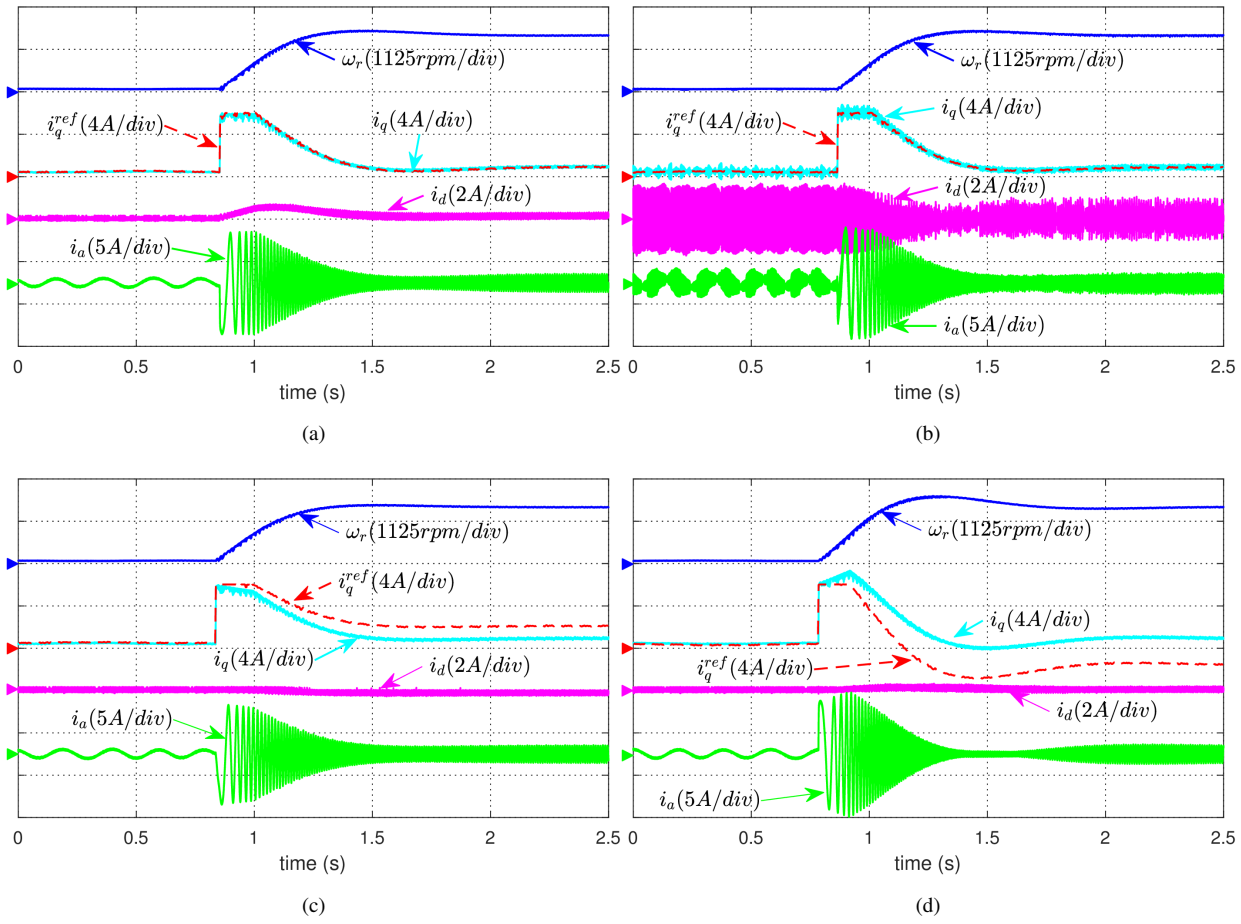

Fig. 5. Responses of conventional DBPC with mismatched parameters: (a) $\hat{L}_s = 0.5L_s$, (b) $\hat{L}_s = 2L_s$, (c) $\hat{\psi}_r = 0.5\psi_r$ and (d) $\hat{\psi}_r = 2\psi_r$.

where $\hat{u}_{d\alpha}$ and $\hat{u}_{d\beta}$ are real and imaginary part of $\hat{\boldsymbol{u}}_d$ respectively. As explained previously, $\hat{\boldsymbol{u}}_d$ is the result of $\boldsymbol{u}_d$ passing a complex coefficient, which can attenuate noises and harmonics. Hence, phase-locked loop (PLL) is not compulsory for the proposed SMDO. After obtaining rotor position, rotor speed can be directly calculated as

$$\hat{\omega}_r^k = \frac{\hat{\theta}_r^k - \hat{\theta}_r^{k-1}}{T_{sp}} \tag{45}$$

To reduce noise-sensitivity, $\hat{\omega}_r^k$ can be filtered by a low-pass filter (LPF) in practical application.

VI. Experimental Results

Experimental tests were carried out on a 2.4 kW PMSM test bench. Motor and control parameters are listed in table I. The developed algorithm is implemented on a 32-bit floating point DSP TMS320F28335. All the data of waveforms are acquired by a Yologawa's DL850E scopecorder. During experimental tests, a magnetic powder brake is used to apply external load to the tested motor. Detailed experimental setup is shown in Fig. 4.

TABLE I

MACHINE AND CONTROL PARAMETERS

DC-bus voltage	U_{dc}	540 V
Rated power	P_N	2.4 kW
Rated voltage	U_N	380 V
Rated frequency	f_N	100 Hz
Number of pole pairs	N_p	4
Stator resistance	R_s	2.25 Ω
Inductance	L_s	23.45 mH
Rotor flux	ψ_r	0.4 Wb
Control period	T_{sp}	100 μs
SMDO parameter 1	λ_{min}	800
SMDO parameter 2	l	1200
SMDO parameter 3	ω_c	1500

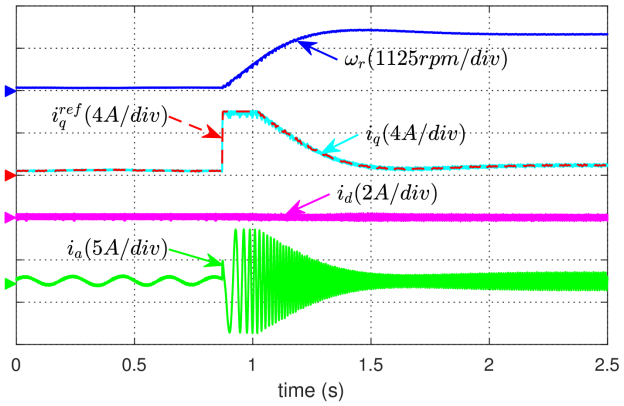

(a)

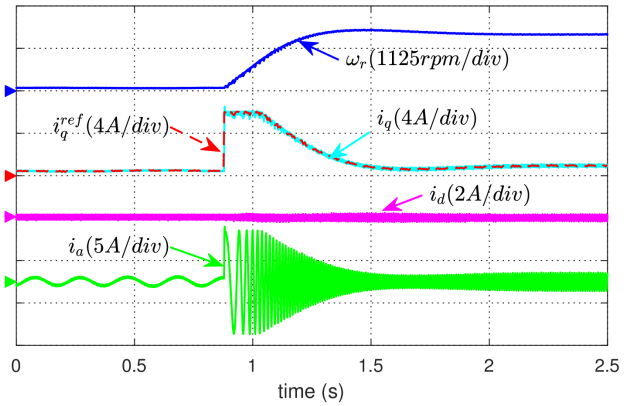

(b)

Fig. 6. Robust DBPC with mismatched parameters: (a) $\hat{L}_s = 2L_s$ and (b) $\hat{L}_s = 0.5L_s$.

A. Roubstness Test of SMDO based DBPC

Figs. 5 and 6 illustrate performance comparisons of conventional DBPC and robust DBPC under different parameter errors. In those tests, the motor is initially running at 75 rpm. Then, the speed command steps to rated value 1500 rpm.

Fig. 5 shows the responses of conventional DBPC with inaccurate inductance and rotor flux. The stator inductance $\hat{L}_s$ and rotor flux $\hat{\psi}_r$ used in the controller are set as $0.5L_s$, $2L_s$, $0.5\psi_r$ and $2\psi_r$ respectively. With a underestimated inductance, i_d would deviate from its reference when i_q is not zero, as seen in Fig. 5(a). With a overestimated inductance, significant ripple components can be seen in both waveforms of i_d and i_q, as shown in Fig. 5(b). With inaccurate rotor flux, the tracking error of i_q gradually gets larger along with the increase of rotor speed, as seen in Figs. 5(c) and 5(d). These results confirm performance deterioration of conventional DBPC under mismatched parameters.

By comparison, DBPC based on the proposed SMDO can still track current references accurately despite inaccurate motor parameters. It is seen in (42) that the proposed DBPC doesn't rely on the knowledge of rotor flux. Additionally, stator resistance has less impact on control performance. As a result, inductance is only concerned parameter in the proposed DBPC and its robustness are tested by setting $\hat{L}_s = 0.5L_s$ and $\hat{L}_s = 2L_s$. The result is shown in Fig. 6. When inductance is underestimated, i_d can still be kept at zero without being influenced by i_q. For a overestimated inductance, there is no large ripples like that in Fig. 5(b). The test result validates that satisfactory tracking performance can be guaranteed under mismatched parameters by the proposed DBPC.

B. Position-Sensorless Operation

As explained in section V-B, the proposed SMDO can be used for position-sensorless control with refined estimation of motor parameters. In the following tests, actual position and speed are acquired through an optical encoder. They are not used in the controller or observer, but only displayed in the scope for checking the accuracy of the estimation. Fig. 7 shows steady state responses with rated load at 1500 rpm (100% rated speed) and 75 rpm (5% rated speed). It is seen that the estimated position almost coincides with the actual position. There is no chattering phenomenon or significant ripples though the position is directly calculated through arc-tangent function. This test show that the designed observer can work well at both low speed and high speed.

Fig. 8 shows experimental results when a rated external load is applied and then released at rated speed. In the figure, $\Delta\omega_r = \omega_r - \hat{\omega}_r$ is estimation error of rotor speed and $\Delta\theta_r = \theta_r - \hat{\theta}_r$ is estimation error of rotor position. It is seen that $\Delta\theta_r$ is small and there is no large speed error during dynamic process. The actual rotor speed can return to its reference quickly after load change, indicating good robustness against load variation.

Fig. 9 shows tested responses during speed variation. Initially, the motor is rotating at 150 rpm. After a moment, speed reference steps to 1500 rpm and then returns to 150 rpm. It can be seen that the actual speed can track the reference quickly and the controller can work stably during fast speed change (4500 rpm/s). As back-EMF is small during low speed operation, the observer is more sensitive to non-ideal factors, such as deadtime, noises and DC bias in the measurement. As a result, the harmonic errors get larger as speed decreases. Nevertheless, the average

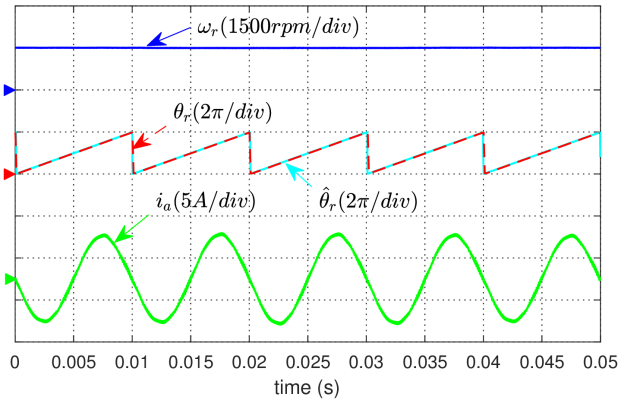

(a)

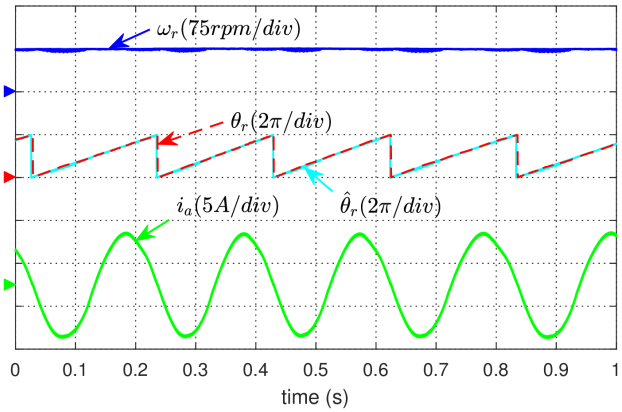

(b)

Fig. 7. Steady state responses of position-sensorless control with rated load at (a) 1500 rpm and (b) 75 rpm.

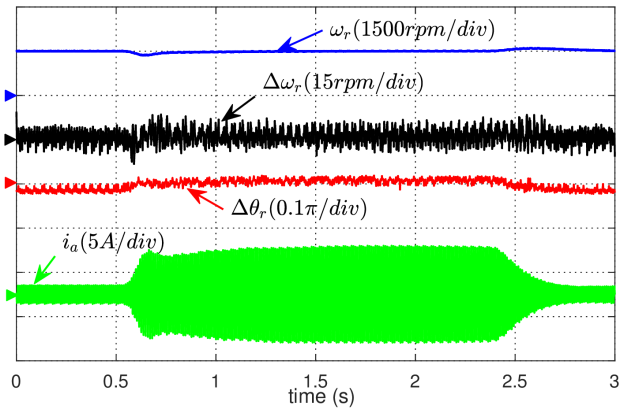

Fig. 8. Responses to step load disturbance at 1500 rpm.

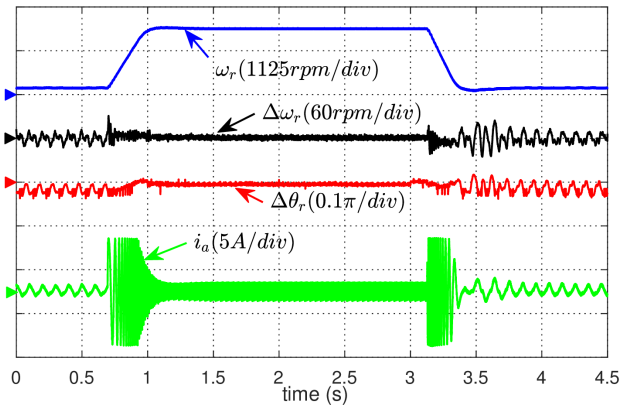

Fig. 9. Responses during speed variation from 150 rpm to 1500 rpm and then to 150 rpm.

estimation error of rotor speed is zero during stead state and there is no excessive position error during fast speed variation.

VII. Conclusion

A multipurpose SMDO is designed and verified by experimental tests in this paper, which can achieve either robust current control or position-sensorless control. Theoretical analysis based on the concept of complex vector shows that the proposed SMDO can accurately estimate disturbance resulting from mismatched parameters and back-EMF. As a complex-coefficient filter is inherently embedded in the proposed SMDO, there is no high frequency chattering problem and a smooth estimation of disturbance voltage can thus be obtained. Based on the proposed SMDO, the developed DBPC is non-sensitive to inaccurate knowledge of stator inductance and rotor flux when position information is available. Additionally, with sophisticated offline-commission, the proposed SMDO can be used as a position estimator for sensorless control. Experimental results on both robustness test and sensorless operation validate the analysis and effectiveness of the proposed control system.

Appendix

Subtracting (8) from (3) yields

$$\hat{\boldsymbol{i}}_s^{k+1} = \frac{L_s \boldsymbol{i}_s^{k+1} + (\Delta R \cdot T_{sp} - \Delta L)\boldsymbol{i}_s^k + j\omega_r^k T_{sp} \cdot \Delta\psi e^{j\theta_r^k}}{\hat{L}_s} \tag{46}$$

According to (3) and (9), actual stator current at $(k+2)$th instant can be expressed as

$$\begin{aligned} L_s \boldsymbol{i}_s^{k+2} = {} & \hat{L}_s \boldsymbol{i}_{ref}^{k+2} + L_s \boldsymbol{i}_s^{k+1} - \hat{L}_s \hat{\boldsymbol{i}}_s^{k+1} \\ & + T_{sp}(\hat{R}_s \hat{\boldsymbol{i}}_s^{k+1} - R_s \boldsymbol{i}_s^{k+1}) - j\omega_r^k T_{sp} \cdot \Delta\psi e^{j\theta_r^{k+1}} \end{aligned} \tag{47}$$

Substituting (46) into (47) yields

$$\begin{aligned} L_s\boldsymbol{i}_s^{k+2} &= \hat{L}_s\boldsymbol{i}_{ref}^{k+2} + (\frac{\hat{R}_s}{\hat{L}_s}\Delta L - \Delta R)T_{sp}\boldsymbol{i}_s^{k+1} \\ &+ (\Delta L - \frac{\hat{R}_s}{\hat{L}_s}\Delta L \cdot T_{sp} - \Delta R \cdot T_{sp})\boldsymbol{i}_s^k \\ &- j\omega_r^k T_{sp} \cdot \Delta\psi(e^{j\theta_r^k} + e^{j\theta_r^{k+1}}) \\ &+ \frac{\hat{R}_s}{\hat{L}_s}(\Delta R\boldsymbol{i}_s^k + j\omega_r^k\Delta\psi e^{j\theta_r^k}) \cdot T_{sp}^2 \end{aligned} \tag{48}$$

Neglecting T_{sp}^2 related terms, and multiplying (48) by $e^{-j\theta_r^{k+2}}$ to transform stator current into synchronous reference frame, the following equations can be obtained

$$\begin{aligned} L_s\boldsymbol{i}_{dq}^{k+2} &= \hat{L}_s\boldsymbol{i}_{dq}^{ref} + (\frac{\hat{R}_s}{\hat{L}_s}\Delta L - \Delta R)T_{sp}\boldsymbol{i}_{dq}^{k+1} \cdot c \\ &+ (\Delta L - \frac{\hat{R}_s}{\hat{L}_s}\Delta L \cdot T_{sp} - \Delta R \cdot T_{sp})\boldsymbol{i}_{dq}^k \cdot c^2 \\ &- j\omega_r^k T_{sp} \cdot \Delta\psi(c^2 + c) \end{aligned} \tag{49}$$

where $c = e^{-j\omega_r T_{sp}} \approx 1 - j\omega_r T_{sp}$. Rewriting (49) into scalar components yields

$$\begin{aligned} L_s i_d^{k+2} &= \hat{L}_s i_{dref}^k + T_{sp}(\frac{\hat{R}_s}{\hat{L}_s}\Delta L - \Delta R)(i_d^{k+1} + \omega_r T_{sp} \cdot i_q^{k+1}) \\ &+ (\Delta L - \frac{\hat{R}_s}{\hat{L}_s}\Delta L \cdot T_{sp} - \Delta R \cdot T_{sp})(i_d^k + 2\omega_r T_{sp} \cdot i_q^k) \\ &- 3(\omega_r T_{sp})^2\Delta\psi \end{aligned} \tag{50}$$

$$\begin{aligned} L_s i_q^{k+2} &= \hat{L}_s i_{qref}^k + T_{sp}(\frac{\hat{R}_s}{\hat{L}_s}\Delta L - \Delta R)(i_q^{k+1} - \omega_r T_{sp} \cdot i_d^{k+1}) \\ &+ (\Delta L - \frac{\hat{R}_s}{\hat{L}_s}\Delta L \cdot T_{sp} - \Delta R \cdot T_{sp})(i_q^k - 2\omega_r T_{sp} \cdot i_d^k) \\ &- 2\omega_r T_{sp} \cdot \Delta\psi \end{aligned} \tag{51}$$

REFERENCES

[1] B.-H. Bae and S.-K. Sul, "A compensation method for time delay of full-digital synchronous frame current regulator of PWM AC drives," *IEEE Trans. Ind. Appl.*, vol. 39, no. 3, pp. 802–810, 2003.

[2] J. W. Jung, Y. S. Choi, V. Q. Leu, and H. H. Choi, "Fuzzy pi-type current controllers for permanent magnet synchronous motors," *IET Electr. Power Appl.*, vol. 5, no. 1, pp. 143–152, January 2011.

[3] W. Wang, J. Zhang, and M. Cheng, "A dual-level hysteresis current control for one five-leg vsi to control two pmsms," *IEEE Trans. Power Electron.*, vol. 32, no. 1, pp. 804–814, Jan 2017.

[4] A. N. Tiwari, P. Agarwal, and S. P. Srivastava, "Performance investigation of modified hysteresis current controller with the permanent magnet synchronous motor drive," *IET Electr. Power Appl.*, vol. 4, no. 2, pp. 101–108, February 2010.

[5] S. H. Chang, P. Y. Chen, Y. H. Ting, and S. W. Hung, "Robust current control-based sliding mode control with simple uncertainties estimation in permanent magnet synchronous motor drive systems," *IET Electr. Power Appl.*, vol. 4, no. 6, pp. 441–450, July 2010.

[6] X. Zhang, B. Hou, and Y. Mei, "Deadbeat predictive current control of permanent-magnet synchronous motors with stator current and disturbance observer," *IEEE Trans. Power Electron.*, vol. 32, no. 5, pp. 3818–3834, May 2017.

[7] M. Siami, D. A. Khaburi, A. Abbaszadeh, and J. Rodríguez, "Robustness improvement of predictive current control using prediction error correction for permanent-magnet synchronous machines," *IEEE Trans. Ind. Electron.*, vol. 63, no. 6, pp. 3458–3466, June 2016.

[8] H. Yang, Y. Zhang, P. D. Walker, J. Liang, N. Zhang, and B. Xia, "Speed sensorless model predictive current control with ability to start a free running induction motor," *IET Electr. Power Appl.*, vol. 11, no. 5, pp. 893–901, 2017.

[9] A. G. Yepes, A. Vidal, J. Malvar, O. Lòpez, and J. Doval-Gandoy, "Tuning method aimed at optimized settling time and overshoot for synchronous proportional-integral current control in electric machines," *IEEE Trans. Power Electron.*, vol. 29, no. 6, pp. 3041–3054, June 2014.

[10] F. Sebaaly, H. Vahedi, H. Y. Kanaan, N. Moubayed, and K. Al-Haddad, "Sliding mode fixed frequency current controller design for grid-connected npc inverter," *IEEE J. Emerg. Sel. Topics Power Electron.*, vol. 4, no. 4, pp. 1397–1405, Dec 2016.

[11] C. Martín, M. R. Arahal, F. Barrero, and M. J. Durán, "Five-phase induction motor rotor current observer for finite control set model predictive control of stator current," *IEEE Trans. Ind. Electron.*, vol. 63, no. 7, pp. 4527–4538, July 2016.

[12] T. Wang, C. Liu, G. Lei, Y. Guo, and J. Zhu, "Model predictive direct torque control of permanent magnet synchronous motors with extended set of voltage space vectors," *IET Electr. Power Appl.*, vol. 11, no. 8, pp. 1376–1382, 2017.

[13] T. Geyer and D. Quevedo, "Multistep finite control set model predictive control for power electronics," *IEEE Trans. Power Electron.*, vol. 29, no. 12, pp. 6836–6846, Dec 2014.

[14] Y. Zhang, B. Xia, and H. Yang, "Performance evaluation of an improved model predictive control with field oriented control as a benchmark," *IET Electr. Power Appl.*, vol. 11, no. 5, pp. 677–687, 2017.

[15] C. Xia, M. Wang, Z. Song, and T. Liu, "Robust model predictive current control of three-phase voltage source PWM rectifier with online disturbance observation," *IEEE Trans. Ind. Informat.*, vol. 8, no. 3, pp. 459–471, 2012.

[16] S. A. Davari, D. A. Khaburi, F. Wang, and R. M. Kennel, "Using full order and reduced order observers for robust sensorless predictive torque control of induction motors," *IEEE Trans. Power Electron.*, vol. 27, no. 7, pp. 3424–3433, July 2012.

[17] S. K. Tseng, T. H. Liu, and J. L. Chen, "Implementation of a sensorless interior permanent magnet synchronous drive based on current deviations of pulse-width modulation switching," *IET Electr. Power Appl.*, vol. 9, no. 2, pp. 95–106, 2015.

[18] S. y. Kuai, S. Zhao, F. p. Heng, and X. Cui, "Position sensorless technology of switched reluctance motor drives including mutual inductance," *IET Electr. Power Appl.*, vol. 11, no. 6, pp. 1085–1094, 2017.

[19] S. K. Kommuri, M. Defoort, H. R. Karimi, and K. C. Veluvolu, "A robust observer-based sensor fault-tolerant control for pmsm in electric vehicles," *IEEE Trans. Ind. Electron.*, vol. 63, no. 12, pp. 7671–7681, Dec 2016.

[20] S. Po-ngam and S. Sangwongwanich, "Stability and dynamic performance improvement of adaptive full-order observers for sensorless pmsm drive," *IEEE Trans. Power Electron.*, vol. 27, no. 2, pp. 588–600, Feb 2012.

[21] V. Smidl and Z. Peroutka, "Advantages of square-root extended kalman filter for sensorless control of ac drives," *IEEE Trans. Ind. Electron.*, vol. 59, no. 11, pp. 4189–4196, Nov 2012.

[22] Z. Qiao, T. Shi, Y. Wang, Y. Yan, C. Xia, and X. He, "New sliding-mode observer for position sensorless control of permanent-magnet synchronous motor," *IEEE Trans. Ind. Electron.*, vol. 60, no. 2, pp. 710–719, Feb 2013.

[23] M. Comanescu, "Design and implementation of a highly robust sensorless sliding mode observer for the flux magnitude of the induction motor," *IEEE Trans. Energy Convers.*, vol. 31, no. 2, pp. 649–657, June 2016.

[24] H. Yang, Y. Zhang, and N. Zhang, "Two high performance position estimation schemes based on sliding-mode observer for sensorless spmsm drives," in *2016 IEEE 8th International Power Electronics and Motion Control Conference (IPEMC-ECCE Asia)*, May 2016, pp. 3663–3669.

[25] P. Cortes, J. Rodriguez, C. Silva, and A. Flores, "Delay compensation in model predictive current control of a three-phase inverter," *IEEE Trans. Ind. Electron.*, vol. 59, no. 2, pp. 1323–1325, 2012.

[26] W. Gao and J. C. Hung, "Variable structure control of nonlinear systems: a new approach," *IEEE Trans. Ind. Electron.*, vol. 40, no. 1, pp. 45–55, Feb 1993.

[27] G. Wang, L. Qu, H. Zhan, J. Xu, L. Ding, G. Zhang, and D. Xu, "Self-commissioning of permanent magnet synchronous machine drives at standstill considering inverter nonlinearities," *IEEE Trans. Power Electron.*, vol. 29, no. 12, pp. 6615–6627, Dec 2014.